Magnetic X-Ray Imaging Using a Single Polarization and Multimodal Ptychography

Marisel Di Pietro Martínez, Alexis Wartelle, Nicolas Mille, Stefan Stanescu, Rachid Belkhou, Farid Fettar, Vincent Favre-Nicolin, Guillaume Beutier

Magnetic X-ray imaging using a single polarization and multimodal-ptychography

Marisel Di Pietro Martínez,[1, 2, *] Alexis Wartelle,[1, 3, 4] Nicolas Mille,[5] Stefan Stanescu,[5] Rachid Belkhou,[5] Farid Fettar,[4] Vincent Favre-Nicolin,[3] and Guillaume Beutier[1]

[1] *Univ. Grenoble Alpes, CNRS, Grenoble INP, SIMaP, 38000 Grenoble, France*
[2] *Max Planck Institute for Chemical Physics of Solids, Noethnitzer Str. 40, 01187 Dresden, Germany*
[3] *European Synchrotron Radiation Facility, F-38043 Grenoble, France*
[4] *Univ. Grenoble Alpes, CNRS, Institut Néel, 38042 Grenoble, France*
[5] *Synchrotron SOLEIL, Saint Aubin, BP 48, 91192 Gif-sur-Yvette, France*

(Dated: August 7, 2024)

Polarized X-rays allow for imaging birefringent or dichroic properties of materials with nanometric resolution. To disentangle these properties from the electronic density, either a polarization analyzer or several measurements with different polarizations (typically two, or more) are needed. Here we demonstrate that ptychography can disentangle these from a single-polarization measurement by using a multimodal analysis. This new method provides an alternative to obtain polarization-resolved images of a sample when manipulating the incident polarization is not possible nor sufficient.

INTRODUCTION

Since their discovery, X-rays have been recognized for their potential in microscopy [1]. Many imaging modes have been developed, in full-field or in scanning mode, with or without lenses, using various contrast mechanisms such as absorption [1], fluorescence [2], phase contrast [3], diffraction [4, 5], etc. In particular, using polarized X-rays and combining measurements with different polarizations allows for evidencing the dichroism [6–8] and birefringence [9, 10] of materials, whether they are of structural [7, 9, 10] or magnetic [6, 11] origin. Dichroic materials absorb the light in different amounts depending on the light polarization, *i.e.* they present a difference between the absorption coefficients of two orthogonal polarizations, while birefringent materials rotate the polarization plane differently depending on the polarization of the incident light, showing a difference between the refractive indices of two orthogonal polarizations [12]. Linear birefringence or dichroism is obtained by combining measurements with two orthogonal linear polarizations, while circular birefringence or dichroism is obtained by combining measurements with two orthogonal circular polarizations [12]. In magnetism, linear birefringence or dichroism is usually used to evidence the magnetization component that is perpendicular to the direction of propagation of the incident light, while circular birefringence or dichroism is used to evidence the magnetization component that is parallel to this direction [12].

While controlling the polarization of the incident photons is nowadays fairly easy, in particular with synchrotron radiation [13, 14], analyzing the polarization of X-rays after their interaction with the sample remains a difficult task. This is particularly true for most imaging methods, since they rely on the use of 2D detectors (with the notable exception of scanning microscopies that can be performed with a point detector). The usual way to analyze the polarization of X-rays is to diffract them at 90° from a crystal or an artificial grating with a period tuned for their wavelength, according to Bragg's law [15, 16]: an azimuthal scan of the analyzer around the propagation axis allows to fully determine the Stoke polarization parameters [17]. This procedure assumes a well defined propagation axis, which is not always the case when measuring with an area detector pointing at a small sample. When the angular spread of X-rays exceed the angular acceptance of the analyzer, its efficiency becomes inhomogeneous, altering the quality of recorded images. It is nevertheless of great interest to perform a polarization analysis of X-rays after the sample since the change of polarization in the sample carry important information [18, 19].

Ptychography is a microscopy technique based on the combination of direct-space scanning and reciprocal-space intensity measurements with a coherent beam [20–25]. It benefits from high spatial resolution and retrieves the complex exit wave allowing for both amplitude and phase contrast. Interestingly, thanks to the redundancy of information measured in a ptychographic data set, more information than a single image of the sample can be recovered. This property is often also used to retrieve an image of the probe illuminating the sample [26], or the true positions of the beam with respect to the sample during the scan [27].

Going further, Thibault *et al.* pointed out that ptychography is able to disentangle several waves exiting the sample without interfering, *i.e.* mutually incoherent, which reduce the interference contrast in the scattering patterns measured at each point of the scan [28]. This incoherence can be either due to the partial coherence of the incident beam, a very common case, but also to a mixture of orthogonal states in the sample. The key idea is that X-rays exiting the sample can be considered as a mixture of coherent but mutually incoherent waves, regardless of the reason why they are not interfering. It is for instance the case when the sample fluctuates at timescales below the timescale of the measurements [29, 30]. Another possible reason for two electro-

magnetic waves not to interfere is if they have orthogonal polarizations. The latter can be linear, or circular, or more generally, elliptical. Therefore, ptychography should be able to disentangle exit waves with orthogonal polarizations, overcoming the aforementioned usual limitations in the X-ray polarization analysis. To demonstrate this, here we show the case of magnetic materials in which the magnetic texture can be disentangled from the electronic structure, from a single ptychographic measurement with incident linear polarization.

MULTIMODAL FORMULATION

In ptychography, for each positioning of the beam relative to the sample, a diffraction pattern is measured with the detector, as illustrated in Fig. 1. The key of this technique is the overlapping of the illuminated areas (see Fig. 1, right-lower corner). This results in redundancy of the data which allows a robust reconstruction of a wide field of view of the sample. The resulting set of diffraction intensities can be used to recover the complex transmitted or exit wave.

To derive the multimodal formulation in this context, let us calculate the transmission of a polarized incident wave $\vec{E}_0 = \Psi_0 \hat{\epsilon}$ defined by its complex amplitude Ψ_0 and its polarization $\hat{\epsilon}$. When $\hat{\epsilon}$ is an eigenvector of the polarization-dependent transmission function, *i.e.* the polarization is not modified through the sample, the transmitted complex amplitude can be written as:

$$\Psi = \Psi_0 \exp\left(\frac{2\pi i}{\lambda}\int n \mathrm{d}z\right), \tag{1}$$

where λ is the wavelength, the wave propagates along the z axis, and $n = n(x, y, z)$ is the optical index. When $\hat{\epsilon}$ is not an eigenvector of the polarization-dependent transmission function, the wave can always be decomposed on a polarization basis of eigenvectors $\vec{E} = \Psi_1\hat{\epsilon}_1 + \Psi_2\hat{\epsilon}_2$ such that Eq. 1 applies independently to both components with different optical indices.

In ferromagnetic materials with isotropic local structure, circular polarizations are such eigenvectors. The optical index can then be expressed as $n = n_c \pm n_m$, where n_c and n_m denote the contribution from the electronic and the magnetic structure, respectively, and the change in sign depends on the helicity of the polarization. Therefore, in this case, Eq. 1 leads to

$$\Psi^{\pm} = \Psi_c \exp\left(\pm\frac{2\pi i}{\lambda}\int n_m \mathrm{d}z\right), \tag{2}$$

where Ψ^+ and Ψ^- correspond to the exit waves for right and left circular polarization, respectively, and

$$\Psi_c = \Psi_0 \exp\left(\frac{2\pi i}{\lambda}\int n_c \mathrm{d}z\right). \tag{3}$$

We can isolate the magnetic part of the optical index by calculating the ratio $\frac{\Psi^+}{\Psi^-}$, which leads to:

$$\arg\left(\frac{\Psi^+}{\Psi^-}\right) \propto \delta_m, \tag{4}$$

$$\ln\left|\frac{\Psi^+}{\Psi^-}\right| \propto \beta_m. \tag{5}$$

where δ_m and β_m are the real and imaginary parts of n_m, respectively. Eq. 4 corresponds to what is known as the phase contrast and Eq. 5 corresponds to the amplitude contrast. Similarly, we can access the electronic contribution to the optical index by calculating the product $\Psi^+\Psi^-$, which results in

$$\arg\left(\Psi^+\Psi^-\right) \propto \delta_c + C_1, \tag{6}$$

$$\ln\left|\Psi^+\Psi^-\right| \propto \beta_c + C_2, \tag{7}$$

where δ_c and β_c are the real and imaginary parts of n_c, respectively, and C_1 and C_2 are constants.

Combining ptychography in the small angle scattering geometry with X-ray magnetic circular dichroism (XMCD) allows for probing either δ_m or β_m which in turn are proportional to the magnetic component that is parallel to the beam direction, that is m_z according to the

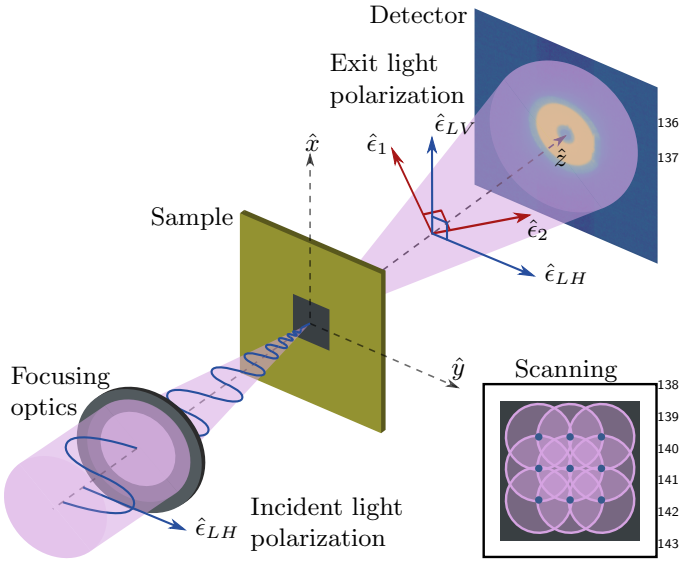

FIG. 1. Ptychography setup: Coherent X-rays illuminate an area of the sample and a diffraction pattern is measured in the far field by a detector. The sample is scanned following a mesh that ensures overlapping illumination, as illustrated in the lower right inset, providing the data redundancy required for a robust image reconstruction. Polarized light provides contrast for dichroic or birefringent samples. $\hat{\epsilon}_{LH}$ and $\hat{\epsilon}_{LV}$ represent the eigenvectors for linearly horizontal and vertical polarized light, respectively, while $\hat{\epsilon}_1$ and $\hat{\epsilon}_2$ represent an alternative orthogonal base for the polarizations.

reference frame defined in Fig. 1. XMCD-ptychography consists on performing one measurement for each helicity of the circular polarization [25, 31, 32], and then, by using Eqs. 4 or 5, an image of the magnetization can be obtained.

In general, we can decompose any polarization vector onto an orthogonal basis of circular polarizations. In particular, in the case of linearly polarized light, this means that we can write the exit wave as the sum of two circularly polarized plane waves

$$\vec{E} = \frac{\sqrt{2}}{2}\left[\Psi^{+}\left(\frac{\hat{\epsilon}_{L1} - i\hat{\epsilon}_{L2}}{\sqrt{2}}\right) + \Psi^{-}\left(\frac{\hat{\epsilon}_{L1} + i\hat{\epsilon}_{L2}}{\sqrt{2}}\right)\right], \quad (8)$$

where $\hat{\epsilon}_{L1}$ and $\hat{\epsilon}_{L2}$ are two orthogonal linear polarizations and the combination $(\hat{\epsilon}_{L1} - i\hat{\epsilon}_{L2})/\sqrt{2}$ and $(\hat{\epsilon}_{L1} + i\hat{\epsilon}_{L2})/\sqrt{2}$ gives us the eigenvectors for right and left circular polarizations, respectively. We can rewrite the previous expression as

$$\vec{E} = \Psi_c\left[\left(\frac{\Psi^{+} + \Psi^{-}}{2}\right)\hat{\epsilon}_{L1} + \left(\frac{\Psi^{+} - \Psi^{-}}{2i}\right)\hat{\epsilon}_{L2}\right]. \quad (9)$$

Since the linear polarizations $\hat{\epsilon}_{L1}$ and $\hat{\epsilon}_{L2}$ are orthogonal, their amplitudes

$$\Psi^{L1} = \Psi_c \cos\left(\frac{2\pi}{\lambda}\int n_m \mathrm{d}z\right) \text{ and} \quad (10)$$

$$\Psi^{L2} = \Psi_c \sin\left(\frac{2\pi}{\lambda}\int n_m \mathrm{d}z\right) \quad (11)$$

do not interfere. Therefore the intensity measured in an experiment with linear polarization can be expressed as the sum of the intensities of these two independent modes

$$I = |\mathcal{F}\{\Psi^{L1}\}|^2 + |\mathcal{F}\{\Psi^{L2}\}|^2, \quad (12)$$

where $\mathcal{F}$ denotes the Fourier transform operator. Here we assume a far-field regime for the detection. However, other operators, like the Fresnel operator, could be consider to account for different propagation regimes. The result from Eq. 12 has previously been used in Ref. [33], for example, to isolate the magnetic term by subtracting two measured diffraction intensities: one with the sample magnetically saturated and another one with the sample not saturated. However, the fact that the two contributions to the intensity can be summed directly suggests they could also be recovered with a multimodal analysis of the ptychography data.

The multimodal approach has been previously shown to be useful for disentangling mixed states of the beam for instance [28], as well as to reconstruct non-orthogonal states in a birefringent liquid crystal with the aid of prior knowledge about the sample [30]. Here we use the multimodal analysis to exploit the orthogonality of the two modes from linear polarization, given by Eqs. 10 and 11, to resolve both the magnetic and the electronic structure from a single ptychographic measurement without any extra constrain.

Calculating the ratio between the modes from Eqs. 10 and 11, and comparing this result to Eqs. 4 and 5, we find the relations

$$2\mathrm{Re}\left[\tan^{-1}\left(\frac{\Psi^{L2}}{\Psi^{L1}}\right)\right] = \arg\left(\frac{\Psi^{+}}{\Psi^{-}}\right) \propto \delta_m, \quad (13)$$

$$2\mathrm{Im}\left[\tan^{-1}\left(\frac{\Psi^{L2}}{\Psi^{L1}}\right)\right] = \ln\left|\frac{\Psi^{+}}{\Psi^{-}}\right| \propto \beta_m, \quad (14)$$

while computing the squared sum of the modes leads to

$$\left(\Psi^{L1}\right)^2 + \left(\Psi^{L2}\right)^2 = \Psi^{+}\Psi^{-} = \Psi_c^2. \quad (15)$$

These equations allow to compare the modes obtained from the single linear polarization with the usual XMCD signal.

EXPERIMENTAL DETAILS

We test the method experimentally on two different samples. We use an Fe/Gd multilayer with nominal stacking of Ta(7)/[Fe(0.7)/Gd(0.7)]$_{60}$/Ta(7) (thickness in nm), and a much thinner sample consisting on a Co/Pt multilayer with nominal stacking of [Co(0.6)/Pt(1)]$_{10}$ (thickness in nm). Both the Fe/Gd and the Co/Pt multilayers were grown on a 300 nm-thick Si_3N_4 membrane suitable for transmission X-ray measurements, and were measured at the peak of absorption at the Fe and Co L_3-edge, respectively.

The ptychography data presented in this work was acquired at HERMES beamline, at SOLEIL synchrotron. Here polarized X-rays are delivered by an helicoidal undulator, allowing to easily switch from horizontal polarization to either of both circular polarizations, with a polarization rate close to 100%. The energy of the photons was tuned by a grating monochromator. The coherence of the beam was ensured by a set of apertures in front of the endstation. The coherent beam was focused using a Fresnel zone plate with 50 nm outer zone width. The sample was placed a few microns downstream the focus in order to obtain a structured illumination that is between 70 and 90 nm wide (see Sec. I of the Supplementary material for more details). The small angle coherent diffraction patterns are acquired on an adapted Tucsen Dhyana 95 sCMOS camera [34] with 2048×2048 pixels of 11 µm. Typical ptychographic datasets were obtained in grid scans with step size of 25 nm and acquisition times of 50 ms per point. The geometrical settings were such that the pixel size of the direct space images is 7 nm.

To analyze the ptychography data, we use PyNX, a Python-based high performance toolkit for coherent X-ray imaging data [35]. For the inversion, we model the beam by a single probe, while the object was associated to two sample modes, these three quantities being further

retrieved from the intensity information. The first mode is initialized with random positive real numbers and the second one with random complex numbers to induce a better separation of the charge and magnetic parts into the first and second modes, respectively (see Sec. III of the Supplementary material for more details). Then, we run 100 iterations of the difference map algorithm, 50 iteration of the alternating projections algorithm, and finally 150 iterations of the maximum likelihood algorithm. The reconstruction is achieved by iterating between the real-space estimated object and the Fourier-space where the amplitude is constrain to the measured diffraction intensity.

EXPERIMENTAL DEMONSTRATION

To demonstrate the method, we started measuring different areas of $1 \times 1\,\mu m^2$ in the Co/Pt film where the electronic density is uniform. In Fig. 2, the pairs (a)-(b), (c)-(d) and (e)-(f) show three of these different areas in the sample. First, we performed an XMCD-ptychography using both left and right circular polarization to use for comparison and verification. For each polarization, we reconstructed the corresponding object using the ptychography algorithm in PyNX and considering one mode for the object and the probe each. We calculate the amplitude contrast following Eq. 5 to probe the out-of-plane magnetization in the thin film. This can be observed on the left side of Fig. 2, *i.e.* (a), (c) and (e). There, worm-like domains of approximately 110 nm wide can be observed for three different areas of the film.

Then, we measured a single linear-polarization ptychography in the same areas. In this case, reconstructing the object with only one mode results in a single and uniform object which represents the electronic density but that is insensitive to the magnetic signal. However, if we enable two modes for the reconstruction of the object, after orthogonalization of the modes [28], and removal of the possible phase ramps and offsets, following Eq. 13, we obtain the magnetic contrast shown on the right panel of Fig. 2, *i.e.* (b), (d) and (f). It can be seen that the magnetic structure recovered by the multimodal analysis matches the one measured by XMCD-ptychography, that is we can recognize the same shapes and distribution of the domains.

With the multimodal approach demonstrated on a sample with uniform electronic structure, we consider now a more complex sample with non-uniform electronic structure. To that end, we took advantage of the structure produced by the carbon deposition on the Fe/Gd sample. In Fig. 3, we show the results for the single linear polarization, and we compare it with those from XMCD-ptychography. Fig. 3(a) and (b) show the contrast for the electronic structure. Two carbon blobs of 52 nm diameter are located in the central area and a larger one of 143 nm in the lower-right corner of the image. These three features can also be seen in the image obtained from the multimodal analysis of the single linear polarization measurement. On the other hand, the magnetic contrast displayed in Fig. 3(c) and (d), shows two opposite domains that are larger than the worm-like domains presented in the previous section. In this case, the single polarization approach has successfully recovered the domain structure. This experiment demonstrates that the multimodal approach can also disentangle more complex electronic structure from the magnetic signal. See Secs. IV and V of the Supplementary material for a discussion on the sensitivity of the technique and the resolution, respectively.

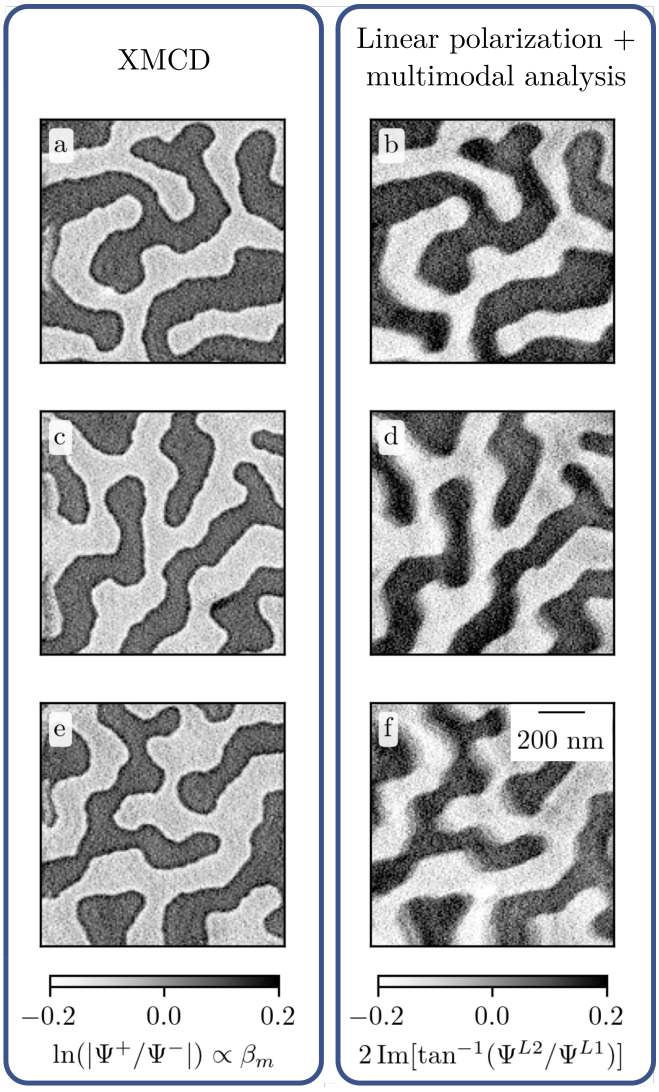

FIG. 2. Comparison between the magnetic contrast imaged by XMCD-ptychography (left) and linear polarization with multimodal analysis (right). Worm-like domains are successfully recovered with both methods in a Co/Pt thin film. The pairs (a)-(b), (c)-(d) and (e)-(f) show three different areas in the sample. The field of view is $1 \times 1\,\mu m^2$.

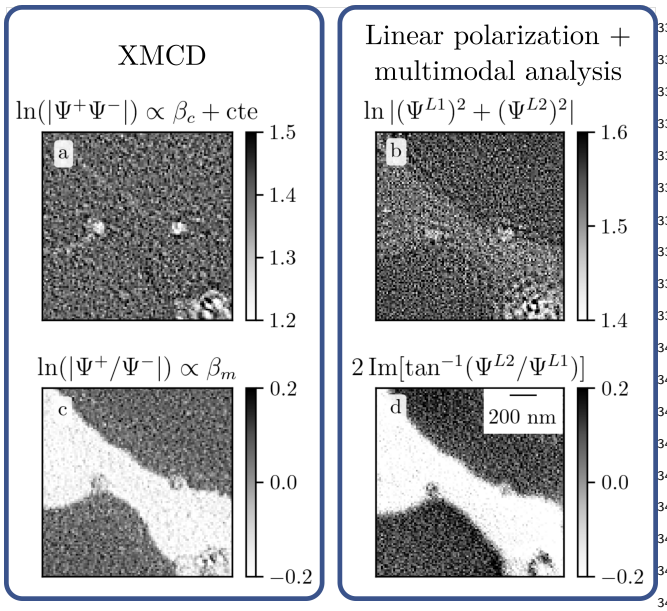

FIG. 3. Comparison between XMCD-ptychography (left) and linear polarization with multimodal analysis (right). (a) and (b) correspond to the electronic contrast. There three blobs of carbon can be resolved on the Fe/Gd surface with both methods. The magnetic contrast, shown in (c) and (d), is also captured with both methods. The field of view is $700 \times 700\,\text{nm}^2$.

DISCUSSION AND CONCLUSIONS

In this work, we demonstrated that, through a multimodal analysis of the reconstructed object, ptychography is able to separate scattered waves with orthogonal polarizations. Specifically, we applied a multimodal analysis to a single ptychographic measurement performed with linear polarization and retrieved two orthogonal object modes. The two modes recovered from our experimental data reproduce the behavior of the charge scattering on the one hand and the magnetic scattering on the other hand, without further data treatment nor constrains from prior knowledge of the sample.

In principle, due to the ambiguity in ptychography using multiple object modes, an unitary transformation [30] can be used to optimize the contrast and the separation of the electronic and magnetic signals (see Sec. II of the Supplementary material for more details on this approach). In the case presented here, the ambiguity corresponds to the arbitrary choice of two orthogonal linear polarizations onto which exit waves are projected: the ptychographic algorithm does not know what is the polarization of the incident wave, and that charge scattering should conserve this polarization. For instance, if the incident polarization is linear horizontal, the set of linear polarizations depicted as $\hat{\epsilon}_1$ and $\hat{\epsilon}_2$ in FIG. 1 is an equivalently good basis from the algorithm point of view. And so would be circular polarizations of opposite helicities, as well as any orthogonal set of elliptical polarizations. However, initializing one of the modes with positive real numbers is sufficient to guide the decomposition into selecting the polarization of charge scattering as one of the vector basis (see Sec. III of the Supplementary material for more details).

Altogether, the capability of ptychography to resolve orthogonal polarizations with a single measurement and without the need of a physical polarization analyzer is of great interest for magnetic imaging. In small angle scattering geometry, as presented here, circular dichroism (or birefringence) remains the most efficient way to extract magnetic contrast, assuming that circular polarization is available. Nevertheless, extracting weak magnetic contrast from circular dichroism relies on a good mutual normalization of the two measurements, which can be difficult in particular when using diffracting quarter-wave plates and on accurate mutual positioning, while the method presented here relies on a single ptychography scan. The method presented here can be extended to image domains in colinear antiferromagnets with magnetic moments aligned along two perpendicular axes in the plane perpendicular to the propagation axis: the single incident polarization has to be chosen circular or linear along the diagonal of the axes of the moments. More importantly, this method could be of great interest for magnetic imaging in a wide angle scattering geometry, for instance in diffraction measurements. Indeed, there is no choice of incident polarization allowing to easily extract the magnetic part of the resonant scattering factor from the charge part [36]. Consequently, it could be an efficient way to image antiferromagnetic textures, including antiphase domains.

Beyond the cases of circular and linear dichroism and birefringence, where the transmission properties of the sample can be described with only two coefficients, there could be a great interest in combining this method with vectorial ptychography [37, 38] for the study of anisotropic media in the most general case: four coefficients are then needed to describe the transmission object, and four measurements with a polarization analyzer are needed; the polarization analyzer could be omitted and only two measurements with different incident polarization would be required. Finally, this method could be applied to other polarized coherent probes than X-rays, and could thus find an application in optical microscopy and specifically in Kerr microscopy.

ACKNOWLEDGMENTS

We acknowledge SOLEIL for providing synchrotron beamtime under project number 20210615. We acknowledge the Agence Nationale de la Recherche for funding under project number ANR-19-CE42-0013-05 and the CNRS for the grant Emergence@INC2020. Computa-

tions were performed on the HPC system Raven at the Max Planck Computing and Data Facility.

* Marisel.DiPietro@cpfs.mpg.de

[1] W. C. Röntgen, On a new kind of rays, Science **3**, 227 (1896).

[2] S. Vogt and A. Lanzirotti, Trends in x-ray fluorescence microscopy, Synchrotron Radiation News **26**, 32 (2013).

[3] M. Endrizzi, X-ray phase-contrast imaging, Nuclear Instruments and Methods in Physics Research Section A: Accelerators, Spectrometers, Detectors and Associated Equipment **878**, 88 (2018), Radiation Imaging Techniques and Applications.

[4] G. A. Chahine, M.-I. Richard, R. A. Homs-Regojo, T. N. Tran-Caliste, D. Carbone, V. L. R. Jacques, R. Grifone, P. Boesecke, J. Katzer, I. Costina, H. Djazouli, T. Schroeder, and T. U. Schülli, Imaging of strain and lattice orientation by quick scanning X-ray microscopy combined with three-dimensional reciprocal space mapping, Journal of Applied Crystallography **47**, 762 (2014).

[5] H. Simons, A. King, W. Ludwig, C. Detlefs, W. Pantleon, S. Schmidt, F. Stöhr, I. Snigireva, A. Snigirev, and H. F. Poulsen, Dark-field x-ray microscopy for multiscale structural characterization, Nature communications **6**, 6098 (2015).

[6] P. Fischer, G. Schütz, G. Schmahl, P. Guttmann, and D. Raasch, Imaging of magnetic domains with the x-ray microscope at bessy using x-ray magnetic circular dichroism, Zeitschrift für Physik B Condensed Matter **101**, 313 (1997).

[7] M. S. Platunov, I. A. Gudim, E. N. Ovchinnikova, K. A. Kozlovskaya, F. Wilhelm, A. Rogalev, A. Hen, V. Y. Ivanov, A. A. Mukhin, and V. E. Dmitrienko, X-ray natural circular dichroism imaging of multiferroic crystals, Crystals **11**, 10.3390/cryst11050531 (2021).

[8] H. Ade and B. Hsiao, X-ray linear dichroism microscopy, Science **262**, 1427 (1993).

[9] B. A. Palmer, G. R. Edwards-Gau, B. M. Kariuki, K. D. Harris, I. P. Dolbnya, and S. P. Collins, X-ray birefringence imaging, Science **344**, 1013 (2014).

[10] Z. Gao, M. Holler, M. Odstrcil, A. Menzel, M. Guizar-Sicairos, and J. Ihli, Nanoscale crystal grain characterization via linear polarization x-ray ptychography, Chem. Commun. **56**, 13373 (2020).

[11] J. Stöhr, A. Scholl, T. Regan, S. Anders, J. Lüning, M. Scheinfein, H. Padmore, and R. White, Images of the antiferromagnetic structure of a nio (100) surface by means of x-ray magnetic linear dichroism spectromicroscopy, Physical Review Letters **83**, 1862 (1999).

[12] A. K. Zvezdin and V. A. Kotov, *Modern Magnetooptics and Magnetooptical Materials*, Condensed Matter Physics (CRC Press, 1997).

[13] S. Sasaki, K. Miyata, and T. Takada, A new undulator for generating variably polarized radiation, Japanese Journal of Applied Physics **31**, L1794 (1992).

[14] C. Giles, C. Vettier, F. de Bergevin, C. Malgrange, G. Grübel, and F. Grossi, X-ray polarimetry with phase plates, Review of Scientific Instruments **66**, 1518 (1995).

[15] S. Chandrasekhar, S. Ramaseshan, and A. K. Singh, Experimental determination of the extinction factor by the use of polarized x-rays, Acta Crystallographica Section A **25**, 140 (1969).

[16] J. B. Kortright, M. Rice, and K. D. Franck, Tunable multilayer EUV/soft x-ray polarimeter, Review of Scientific Instruments **66**, 1567 (1995).

[17] H. Wang, P. Bencok, P. Steadman, E. Longhi, J. Zhu, and Z. Wang, Complete polarization analysis of an APPLE II undulator using a soft X-ray polarimeter, Journal of Synchrotron Radiation **19**, 944 (2012).

[18] C. Mazzoli, S. B. Wilkins, S. Di Matteo, B. Detlefs, C. Detlefs, V. Scagnoli, L. Paolasini, and P. Ghigna, Disentangling multipole resonances through a full x-ray polarization analysis, Phys. Rev. B **76**, 195118 (2007).

[19] Y. L. Wang, G. Fabbris, D. Meyers, N. H. Sung, R. E. Baumbach, E. D. Bauer, P. J. Ryan, J.-W. Kim, X. Liu, M. P. M. Dean, G. Kotliar, and X. Dai, On the possibility to detect multipolar order in uru_2si_2 by the electric quadrupolar transition of resonant elastic x-ray scattering, Phys. Rev. B **96**, 085146 (2017).

[20] W. Hoppe, Principles of electron structure research at atomic resolution using conventional electron microscopes for the measurement of amplitudes and phases, Acta Crystallographica Section A: Crystal Physics, Diffraction, Theoretical and General Crystallography **26**, 414 (1970).

[21] H. M. L. Faulkner and J. Rodenburg, Movable aperture lensless transmission microscopy: a novel phase retrieval algorithm, Physical Review Letters **93**, 023903 (2004).

[22] J. M. Rodenburg, A. Hurst, A. G. Cullis, B. R. Dobson, F. Pfeiffer, O. Bunk, C. David, K. Jefimovs, and I. Johnson, Hard-x-ray lensless imaging of extended objects, Physical Review Letters **98**, 034801 (2007).

[23] P. Thibault, M. Dierolf, A. Men'zel, O. Bunk, C. David, and F. Pfeiffer, High-resolution scanning x-ray diffraction microscopy, Science **321**, 379 (2008).

[24] M. Guizar-Sicairos and P. Thibault, Ptychography: A solution to the phase problem, Physics Today **74**, 42 (2021).

[25] C. Donnelly, V. Scagnoli, M. Guizar-Sicairos, M. Holler, F. Wilhelm, F. Guillou, A. Rogalev, C. Detlefs, A. Menzel, J. Raabe, *et al.*, High-resolution hard x-ray magnetic imaging with dichroic ptychography, Physical Review B **94**, 064421 (2016).

[26] P. Thibault, M. Dierolf, O. Bunk, A. Menzel, and F. Pfeiffer, Probe retrieval in ptychographic coherent diffractive imaging, Ultramicroscopy **109**, 338 (2009).

[27] A. Maiden, M. Humphry, M. Sarahan, B. Kraus, and J. Rodenburg, An annealing algorithm to correct positioning errors in ptychography, Ultramicroscopy **120**, 64 (2012).

[28] P. Thibault and A. Menzel, Reconstructing state mixtures from diffraction measurements, Nature **494**, 68 (2013).

[29] J. N. Clark, X. Huang, R. J. Harder, and I. K. Robinson, Dynamic imaging using ptychography, Phys. Rev. Lett. **112**, 113901 (2014).

[30] P. Li, T. Edo, D. Batey, J. Rodenburg, and A. Maiden, Breaking ambiguities in mixed state ptychography, Optics express **24**, 9038 (2016).

[31] X. Shi, P. Fischer, V. Neu, D. Elefant, J. C. T. Lee, D. A. Shapiro, M. Farmand, T. Tyliszczak, H.-W. Shiu, S. Marchesini, S. Roy, and S. D. Kevan, Soft x-ray ptychography studies of nanoscale magnetic and structural correlations in thin SmCo5 films, Applied Physics Letters **108**, 094103 (2016).

[32] C. Donnelly, M. Guizar-Sicairos, V. Scagnoli, S. Gliga, M. Holler, J. Raabe, and L. J. Heyderman, Three-dimensional magnetization structures revealed with x-ray vector nanotomography, Nature **547**, 328 (2017).

[33] A. Tripathi, J. Mohanty, S. H. Dietze, O. G. Shpyrko, E. Shipton, E. E. Fullerton, S. S. Kim, and I. McNulty, Dichroic coherent diffractive imaging, Proceedings of the National Academy of Sciences **108**, 13393 (2011).

[34] K. Desjardins, K. Medjoubi, M. Sacchi, H. Popescu, R. Gaudemer, R. Belkhou, S. Stanescu, S. Swaraj, A. Besson, J. Vijayakumar, *et al.*, Backside-illuminated scientific cmos detector for soft x-ray resonant scattering and ptychography, Journal of Synchrotron Radiation **27**, 1577 (2020).

[35] V. Favre-Nicolin, G. Girard, S. Leake, J. Carnis, Y. Chushkin, J. Kieffer, P. Paleo, and M.-I. Richard, Pynx: high-performance computing toolkit for coherent x-ray imaging based on operators, Journal of Applied Crystallography **53**, 1404 (2020).

[36] J. Hill and D. McMorrow, Resonant exchange scattering: polarization dependence and correlation function, Acta Crystallographica Section A: Foundations of Crystallography **52**, 236 (1996).

[37] P. Ferrand, M. Allain, and V. Chamard, Ptychography in anisotropic media, Opt. Lett. **40**, 5144 (2015).

[38] Q. Song, A. Baroni, R. Sawant, P. Ni, V. Brandli, S. Chenot, S. Vézian, B. Damilano, P. de Mierry, S. Khadir, *et al.*, Ptychography retrieval of fully polarized holograms from geometric-phase metasurfaces, Nature communications **11**, 2651 (2020).